9D.3 APPLICATION OF ENSEMBLE FORECASTS TO THE STUDY OF TROPICAL CYCLONE INTENSITY: A CASE STUDY OF HURRICANE KATIA (2011)

Rosimar Rios-Berrios * and Ryan D. Torn
Department of Atmospheric and Environmental Sciences
University at Albany, State University of New York, Albany, New York

1. Introduction

Understanding the physical mechanisms leading to the spin up of the low-level winds of tropical cyclones (TCs) could help improve TC intensity forecasts. While several theories have been proposed to explain TC intensification (e.g. Charney and Eliassen 1964; Emanuel 1986; Nguyen et al. 2008), most of these studies have centered on the axisymmetric processes occurring in idealized environments with no background flow. In a real atmosphere, the interaction between small-scale convective processes and the large-scale environment, which is often characterized by vertical wind shear, may lead to different pathways that result in TC intensification. It is thus imperative to study the processes aiding or inhibiting TC spin up within realistic environmental conditions.

With recent advancements in observational and numerical weather prediction systems, it is possible to investigate both the environmental and internal control of TC intensity. One method of studying intensity change is to evaluate composites of multiple cases to determine differences between intensifying and non-intensifying TCs. One of these studies (Hendricks et al. 2010) used global model analyses and satellite-derived data to study the differences associated with the environments of weakening, steady state, intensifying and rapidly intensifying TCs during the period 2003–08. Their results showed that intensifying storms on the North Atlantic and West Pacific were characterized by weaker deep-layer vertical wind shear, higher low- and mid-level relative humidity and warmer sea surface temperature than weakening storms. These findings are consistent with well-recognized favorable environmental conditions for TC intensification. In addition, Rogers et al. (2013) used airborne observations for the period of 1997–2010 to evaluate differences in the inner-core region of intensifying and steady state TCs. Their findings revealed that intensifying TCs had stronger and deeper low-level inflow, stronger vertical motion in the eyewall and a larger number of convective bursts inside the radius of maximum winds. These studies have provided insightful information about the conditions associated with TC intensification; however, both investigations included mature TCs in their weakening or steady state groups, thus making it difficult to apply their results to tropical depressions or tropical storms.

Motivated by the composite approach employed by Hendricks et al. (2010), Rogers et al. (2013) and others, this study also compares composites of intensifying and non-intensifying TCs. Our approach differs from previous studies because we use a large set of high-resolution, full-physics, ensemble forecasts for a particular TC that proved challenging to forecast. Using numerical simulations allows us to study both the environmental and internal contributions to TC intensity changes. The ensemble approach aids in comparing different simulations for the same storm, using the same model physics, but only perturbing the initial conditions. While other studies have also used the ensemble forecasts method to investigate predictability of TC intensity (e.g. Zhang and Sippel 2009; Sippel and Zhang 2010; Torn and Cook 2013), the present study focuses on the storm dynamics rather than on the predictability problem. Our goal is to use the ensemble as a tool to gain a better understanding of the mechanisms that drive TC intensity changes.

2. Methods

2.1. Case study: Hurricane Katia

The case selected for this study is Hurricane Katia, which was a long-lived Atlantic TC that remained over open ocean waters throughout its lifetime (Fig. 1). The genesis of Katia can be tracked back to an African easterly wave that moved over the Eastern Atlantic on 27 August 2011 (Stewart 2012). As the tropical disturbance moved westward, the convection became better organized such that the disturbance was designated a tropical depres-

* *Corresponding author address:* Rosimar Rios-Berrios University at Albany, State University of New York, DAES-ES 325, 1400 Washington Ave., Albany, NY 12222
E-mail: rrios-berrios@albany.edu

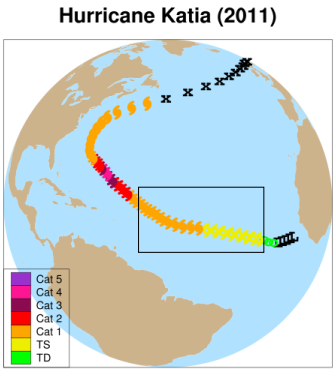

FIG. 1. Best track estimates of Katia's position and intensity (color coded according to the legend). The black box indicates the time period considered in the AHW forecasts.

sion on 0600 UTC 29 August. Despite being influenced by strong vertical wind shear, the tropical depression continued strengthening, becoming Tropical Storm Katia on 0000 UTC 30 August and reaching hurricane intensity 24 hours afterwards (Stewart 2012). The vertical wind shear slightly weakened later on, but a region of dry air emerged from Africa and diminished the tropospheric moisture surrounding the storm. Katia remained at the same intensity for about three days, and numerical models for that period struggled to accurately predict Katia's intensity. It is hypothesized that the dry air surrounding Katia was likely preventing it from intensifying any further.

After overcoming the detrimental effects of shear and dry air, Katia rapidly intensified on 4 September and reached peak intensity on 0000 UTC 6 September (Stewart 2012). The hurricane weakened shortly afterwards as it moved into higher latitudes while recurving on the Western Atlantic. Katia then transitioned into an extratropical cyclone on 10 September when it entered the strong midlatitude flow on the North Atlantic.

2.2. Experimental setup

To investigate the intensity changes of Katia as it developed under the influence of moderate vertical wind shear and dry air, numerical forecasts were produced using the Advanced Hurricane Weather Research and Forecasting model (AHW; Davis et al. 2008). The AHW ensemble system consisted of 96 members generated using a six-hourly cycling ensemble Kalman filter (EnKF) data assimilation technique. The assimilation was done over a 36-km grid spacing domain covering the full Atlantic basin. Whenever a tropical system was designated at least as an INVEST by the National Hurricane Center, the modeling system also assimilated observations into a two-way nested domain with 12-km grid spacing following the tropical system. A free forecast was initialized on 0000 UTC 30 August 2011, which included a third nested domain with 4-km grid spacing that allowed for explicit convection calculation. A description of the assimilated observations and the physical parameterizations used in this modeling system is provided in Torn (2010) and Cavallo et al. (2013).

2.3. Ensemble forecasts diagnosis

The AHW track forecasts captured the general trajectory of Katia, but the intensity forecasts were mixed (Fig. 2). All members were initialized with similar storm intensity based on the minimum sea-level pressure (MSLP) or maximum wind speed (not shown). None of the members predicted the observed intensification of Katia during the first 48 hours of the forecast. More interesting, the ensemble spread at the five-day forecast was quite large and showed a wide range of possible outcomes, ranging from a weak depression to a strong hurricane.

The large variability in the intensity forecast provided an opportunity to study why some members predicted intensification over the five-day period, while other members predicted little or no intensification. In order to answer this question, two subgroups were objectively identified by averaging the MSLP between 48–126 h. The groups selected for comparison were: 1) ten members that predicted the lowest time-averaged MSLP (named strongest members) and 2) ten members that predicted little or no change in MSLP (named weakest members). Composites of these two subgroups were created and compared against each other to discern the differences in the environment and within the vortex. The differences were tested for statistical significance using a bootstrap resampling method on which two subgroups of ten members each were randomly selected and compared against each other. This random resampling was repeated 10,000 times to create a distribution to test the statistical significance of the composite differences between strongest and weakest members.

3. Results

3.1. Uncertainty within the environment

Differences in the TC environment were considered first. Environmental quantities such as SST, 200–850 hPa vertical wind shear, precipitable water vapor (PW), upper level divergence, among oth-

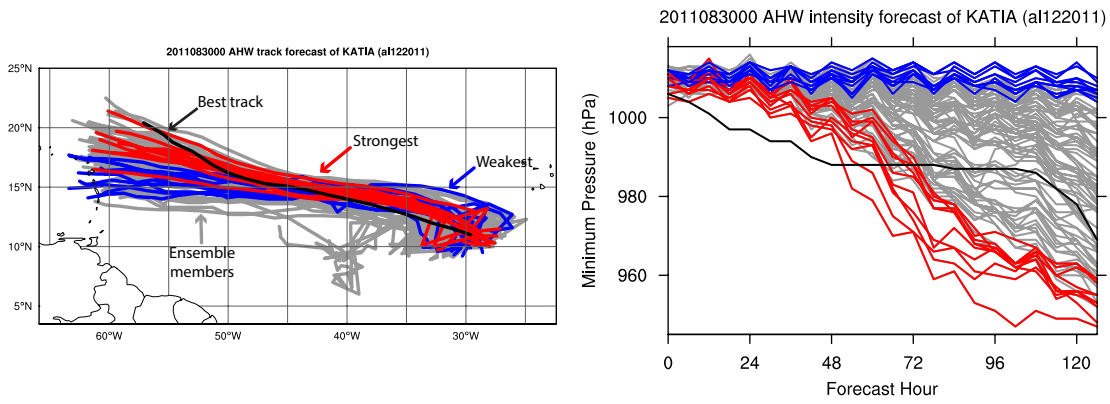

FIG. 2. AHW track (left) and intensity (right) forecasts initialized at 0000 UTC 30 August 2011. The gray lines depict the individual ensemble forecasts while the black line depicts the best track estimates. Red (blue) lines represent the 10 strongest (weakest) members based on the time-averaged minimum sea level pressure.

ers, were averaged within a 500–km radius from the storm center of each ensemble member. The averaging was done to remove the effects of the vortex and evaluate differences associated with the environment itself.

The most interesting differences between the strong and weak members were in wind shear and PW. Fig. 3 shows the normalized joint combination of these two parameters for all members, and also separated for the strongest and weakest members. The joint space for all members show two distinguishable maxima in wind shear. The peak at the higher end was due to the moderate wind shear at the initialization time for all members. The shear difference between the strongest and weakest members was statistically significant only at certain forecast times (e.g. 0 h, 6 h, 18 h, 24 h and 48 h).

When separated into strongest and weakest members, the joint space revealed a preference for PW greater than 56 mm for strongest members, and PW smaller than 56 mm for weakest members. The difference between the mean PW of the strongest and weakest members was found to be statistically significant at the 95% confidence level at all lead times up to 96 h. This result suggests that near-storm environmental water vapor could be important for TC intensification, and the reason for this deserves further investigation.

3.2. Composite differences

To investigate if there was a preferred location and time for differences in PW, horizontal fields in a storm-centered framework were considered. Composites of the strongest and weakest members were computed every six hours. The composite differences revealed that water vapor surrounding the storm was significantly higher in the strongest members beginning at early forecast hours (Fig. 4). At all lead times, the largest differences in PW were located 200–300 km away from the storm center, rather than near the center. Furthermore, the differences in water vapor and moist static energy were largest in the lower troposphere (not shown).

The composite differences of latent heat fluxes showed an asymmetric pattern during the first six hours of the forecast, with evidently large statistically significant differences to the south of the storm center (Fig. 5). With moderate easterly vertical wind shear during the same period (20–25 kts), convection was likely pushed to the west and the enhanced latent heat fluxes in the strongest members were located downwind of the convection. This setup could likely enhance the convection as it rotated counterclockwise with the storm's cyclonic winds. By the 48-h forecast the latent heat fluxes were much higher all around the storm in the strongest members, partially owing to the stronger tangential wind but nevertheless adding more moisture in the lower troposphere and priming the atmosphere for moist convection.

3.3. Water vapor budgets

Having noticed statistically significant differences in PW and latent heat fluxes located far from the storm center, it is worth considering how those differences at relatively large radii produced differences in the inner-core convection and circulation. In an attempt to quantitatively answer this question, water vapor budgets were computed for all members and compared between the strongest and weakest

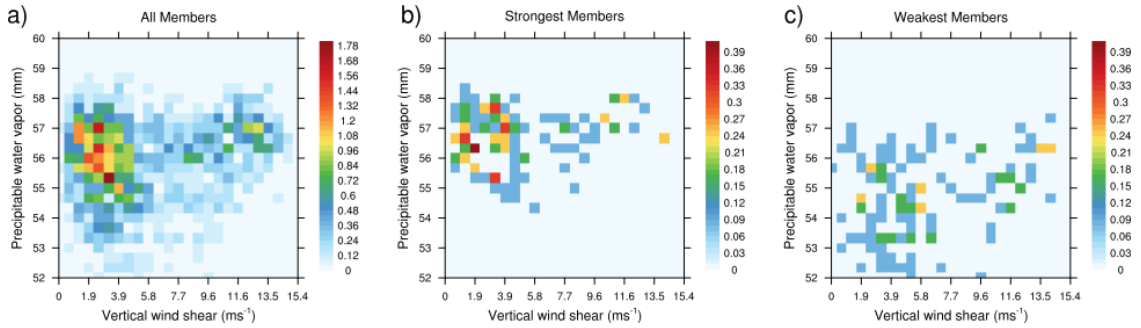

FIG. 3. Joint combinations of precipitable water and vertical wind shear based on the 0–72 h forecasts for (a) all members, (b) strongest members and (c) weakest members. All values are normalized by the total amount of occurrences using all ensemble members.

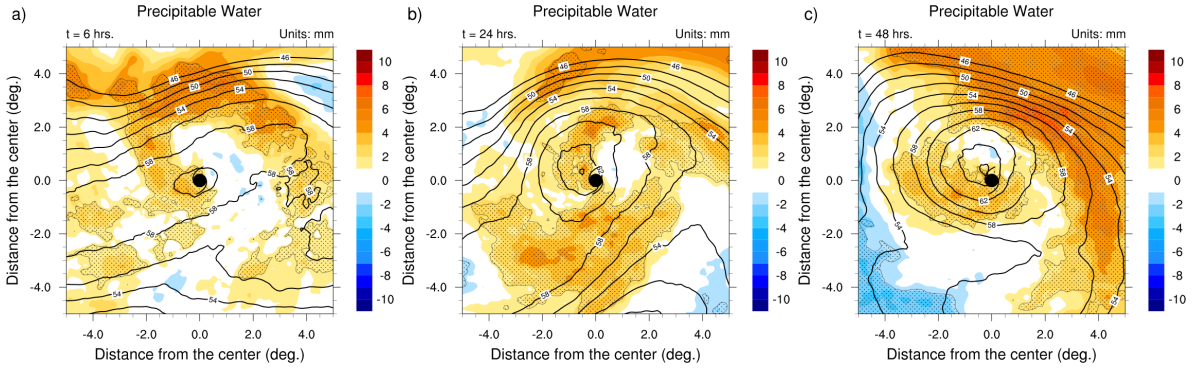

FIG. 4. Storm-centered composite differences of precipitable water between the strongest and weakest members (mm; shaded) at (a) 6 h, (b) 24 h and (c) 48 h. Also shown is the ensemble mean (mm; contours). Stippling pattern indicates statistically significant differences at the 95% confidence level.

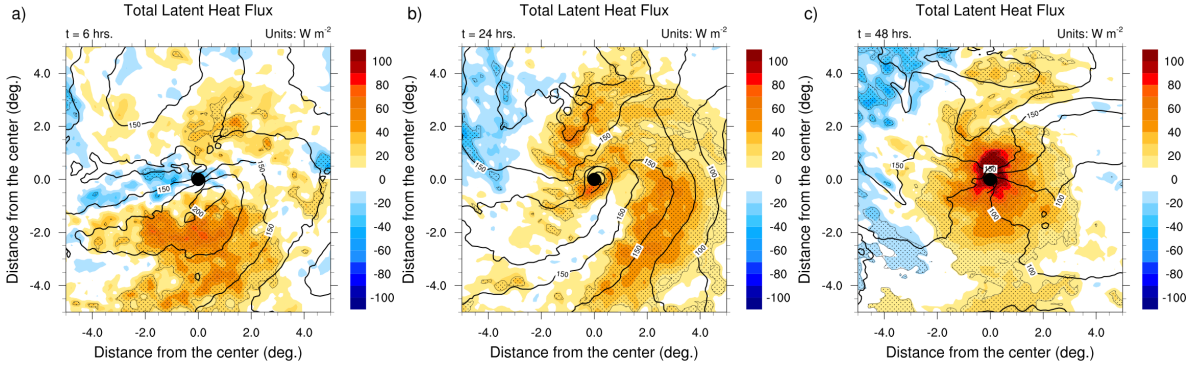

FIG. 5. As in Fig. 4 but for the surface latent heat flux (W m^{-2}).

members. Previous studies have used water vapor budgets to study the storm structure (e.g. Braun 2006), as well as to compare the structure of developing and non-developing TCs (e.g. Fritz and Wang 2013). In the present study we used a similar approach by considering the Boussinesq water vapor equation:

$$\frac{\partial(\rho q_v)}{\partial t} = -\nabla_h \cdot (\rho q_v \vec{V_h}) - \frac{\partial(\rho q_v w)}{\partial z} - C + E + B \quad (1)$$

where q_v is the water vapor mixing ratio, ρ is the dry air density, $\vec{V_h}$ is the horizontal wind, w is the vertical wind speed, C represents condensation, E represents evaporation and B represents the contribution from the planetary boundary layer parameterization scheme. The first two terms to the right hand side of Eq. (1) represent the horizontal and vertical water vapor flux convergence or divergence. These two terms can be used to diagnose the net transport of water vapor towards the storm center and from low- to mid-levels. The terms were averaged over the area of a circle, which by Green's theorem translates into the net flux across the radius of the area considered. Similar to Braun (2006), the budgets were evaluated at two different radii to consider the flux across the inner-core region, and the flux from the environment towards the TC outer region. The first radius, 60 km, was chosen to be 1.5 times the radius of maximum wind of the strongest members at 48 hours. The second radius, 200 km, roughly represents the outermost region of recirculating air as estimated by the closed storm-relative streamlines.

The composite differences of the first two terms of Eq. (1) evaluated at a radius of 60 km are shown in Fig. 6 as a function of height and time. The differences in the first term indicate that the strongest members had greater water vapor flux convergence in the boundary layer, which was statistically significant at all lead times (Fig. 6a). These differences, which reached values of 200 g m^{-3} day^{-1}, first appeared in the initial conditions and persisted throughout the entire forecast period. It is likely that the statistically significantly large differences in latent heat fluxes resulted in more low-level moisture in the strong members. The favorable storm-relative inflow (not shown) could then transport the water vapor towards the storm center, leading to greater horizontal flux convergence in the strongest members.

On the other hand, the vertical water vapor flux term was not statistically significantly different during the first 24 hours of the forecast (Fig. 6b). Even though the boundary layer was moistened by the horizontal flux, there was not enough forcing to promote deep convection. The vertical transport of water vapor became statistically significantly different after 24 hours when a significant amount of water vapor was being transported from the lower to the middle troposphere. This time coincides with the period when the storm in the strongest members slowly started intensifying (Fig. 2). Interestingly, this term was significantly different earlier in the forecast when evaluated at 200 km (not shown). Even though convection was not well organized in the inner-core region, it was aiding in moistening the mid-levels in the outer region.

The evolution of the area-averaged water vapor mixing ratio generally depicts the gradual moistening of the lower troposphere during the first 24 hours of the strongest members forecast (Fig. 6c). The extra moisture extended higher than the layer of enhanced horizontal water vapor flux convergence.

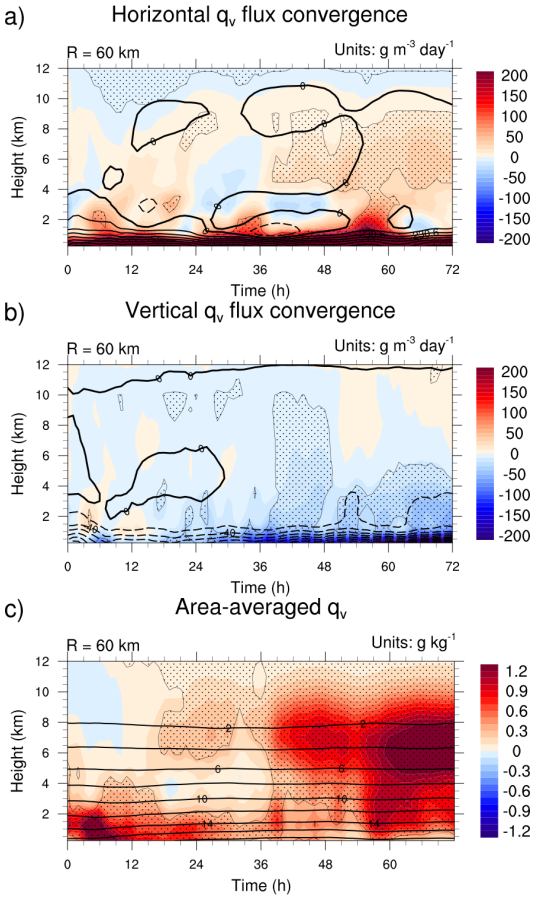

FIG. 6. Composite differences of (a) horizontal water vapor flux convergence, (b) vertical water vapor convergence and (c) area-averaged water vapor mixing ratio (shaded). The black contours depict the ensemble mean and the stippling pattern indicates statistically significant differences at the 90% confidence level.

This result can be attributed to the presence of shallow convection during the 24 h. Once the vertical water vapor flux divergence became significantly different, deep convection and moistening of the middle to upper troposphere occurred in the strongest members, but not in the weakest members. The lack of deep convection in the weakest members did not aid in strengthening the low-level circulation, which is likely the reason why those members remained weak throughout the rest of the forecast.

4. Concluding remarks

A large set of high-resolution, full physics ensemble forecasts was used to investigate TC intensity changes under realistic conditions. The case of Hurricane Katia (2011) was selected for this study based on the challenges numerical models faced in predicting development and intensification. Two distinct groups were identified and compared: 1) ten members that predicted intensification (strongest members) and 2) ten members that did not predict intensification (weakest members). Results showed that a more favorable environment for strengthening with relatively weak vertical wind shear and abundant PW characterized the strongest members. The largest differences in PW were found to be outside the inner-core region of Katia, suggesting that moisture in the near-storm environment is important for development. Stronger latent heat fluxes in the strongest members provided an additional source of boundary layer water vapor. An evaluation of the horizontal and vertical water vapor flux convergence revealed that stronger low-level inward and upward transport of water vapor gradually moistened the middle troposphere, promoting deep convection in the strongest members.

Based on these findings, it is hypothesized that observations of lower tropospheric water vapor and wind field in the near-storm environment may reduce initial condition uncertainty and lead to improved TC intensity forecasts. Future work will evaluate this hypothesis through ensemble-based sensitivity experiments.

5. Acknowledgments

This material is based upon work supported by the National Science Foundation Graduate Research Fellowship under Grant No. DGE 1060277, as well as by the Significant Opportunities in Atmospheric Research and Science (SOARS) program. The authors would like to thank Drs. Christopher Davis and Thomas Auligne for their valuable contributions to this project.

REFERENCES

Braun, S. A., 2006: High-resolution simulation of Hurricane Bonnie (1998). Part II: water budget. *J. Atmos. Sci.*, **63 (1)**, 43–64.

Cavallo, S. M., R. D. Torn, C. Snyder, C. Davis, W. Wang, and J. Done, 2013: Evaluation of the Advanced Hurricane WRF data assimilation system for the 2009 Atlantic hurricane season. *Mon. Wea. Rev.*, **141 (2)**, 523–541.

Charney, J. G. and A. Eliassen, 1964: On the growth of the hurricane depression. *J. Atmos. Sci.*, **21 (1)**, 68–75.

Davis, C., et al., 2008: Prediction of landfalling hurricanes with the advanced hurricane WRF model. *Mon. Wea. Rev.*, **136 (6)**, 1990–2005.

Emanuel, K. A., 1986: An air-sea interaction theory for tropical cyclones. Part I: Steady-state maintenance. *J. Atmos. Sci.*, **43 (6)**, 585–605.

Fritz, C. and Z. Wang, 2013: A numerical study of the impacts of dry air on tropical cyclone formation: A development case and a nondevelopment case. *J. Atmos. Sci.*, **70 (1)**, 91–111.

Hendricks, E. A., M. S. Peng, B. Fu, and T. Li, 2010: Quantifying environmental control on tropical cyclone intensity change. *Mon. Wea. Rev.*, **138 (8)**, 3243–3271.

Nguyen, S. V., R. K. Smith, and M. T. Montgomery, 2008: Tropical-cyclone intensification and predictability in three dimensions. *Q. J. Roy. Meteor. Soc.*, **134 (632)**, 563–582.

Rogers, R., P. Reasor, and S. Lorsolo, 2013: Airborne doppler observations of the inner-core structural differences between intensifying and steady-state tropical cyclones. *Mon. Wea. Rev.*, **141 (9)**, 2970–2991.

Sippel, J. A. and F. Zhang, 2010: Factors affecting the predictability of hurricane Humberto (2007). *J. Atmos. Sci.*, **67 (6)**, 1759–1778.

Stewart, S. R., 2012: Tropical Cyclone Report: Hurricane Katia (AL122011). Tech. rep., National Hurricane Center, 20 pp. [Available online at: http://www.nhc.noaa.gov/data/tcr/AL122011_Katia.pdf].

Torn, R. D., 2010: Performance of a mesoscale Ensemble Kalman Filter (EnKF) during the NOAA High-Resolution Hurricane Test. *Mon. Wea. Rev.*, **138 (12)**, 4375–4392.

Torn, R. D. and D. Cook, 2013: The role of vortex and environment errors in genesis forecasts of Hurricanes Danielle and Karl (2010). *Mon. Wea. Rev.*, **141 (1)**, 232–251.

Zhang, F. and J. A. Sippel, 2009: Effects of moist convection on hurricane predictability. *J. Atmos. Sci.*, **66 (7)**, 1944–1961.